Obrabotka metallov (tekhnologiya, oborudovanie, instrumenty) = Metal Working and Material Science. 2023 vol. 25 no. 4 pp. 216–231
ISSN: 1994-6309 (print) / 2541-819X (online)
DOI: 10.17212/1994-6309-2023-25.4-216-231

NSTU NETI

Obrabotka metallov -
Metal Working and Material Science

Journal homepage: http://journals.nstu.ru/obrabotka_metallov

Influence of high-energy impact during plasma cutting on structure and properties of surface layers of aluminum and titanium alloys

Valery Rubtsov [1, a, *], *Alexander Panfilov* [1, b], *Evgeny Knyazhev* [1, c], *Alexandra Nikolaeva* [1, d], *Andrey Cheremnov* [1, e], *Anastasia Gusarova* [1, f], *Vladimir Beloborodov* [1, g], *Andrey Chumaevskii* [1, h], *Artem Grinenko* [2, i], *Evgeny Kolubaev* [1, k]

[1] Institute of Strength Physics and Materials Science of the Siberian Branch of the RAS, 2/4, pr. Akademicheskii, Tomsk, 634055, Russian Federation
[2] ITS-Siberia LLC, 16a Severnoe Shosse, Krasnoyarsk, 660118, Russian Federation

[a] https://orcid.org/0000-0003-0348-1869, rvy@ispms.tsc.ru; [b] https://orcid.org/0000-0001-8648-0743, alexpl@ispms.ru;
[c] https://orcid.org/0000-0002-1984-9720, clothoid@ispms.tsc.ru; [d] https://orcid.org/0000-0001-8708-8540, nikolaeva@ispms.tsc.ru;
[e] https://orcid.org/0000-0003-2225-8232, amc@ispms.tsc.ru; [f] https://orcid.org/0000-0002-4208-7584, gusarova@ispms.ru;
[g] https://orcid.org/0000-0003-4609-1617, vabel@ispms.tsc.ru; [h] https://orcid.org/0000-0002-1983-4385, tch7av@gmail.com;
[i] https://orcid.org/0009-0002-9511-1303, giga2011@yandex.ru; [k] https://orcid.org/0000-0001-7288-3656, eak@ispms.tsc.ru

ARTICLE INFO

Article history:
Received: 26 September 2023
Revised: 11 October 2023
Accepted: 18 October 2023
Available online: 15 December 2023

Keywords:
Plasma cutting
Ti-4Al-1Mn titanium alloy
Grade2titanium alloy
Macrostructure
Aluminum alloy AA2124
Aluminum alloy AA5056
Heat affected zone
Change of mechanical properties of material

Funding
The results were obtained in the framework of the Integrated Project "Establishment of production of high-tech equipment for adaptive high-precision plasma heavy cutting of non-ferrous metals for the metallurgical, aerospace and transport industries of the Russian Federation" (Agreement No. 075-11-2022-012 dated April 06, 2022) implemented by the ISPMS SB RAS at the financial support of the Ministry of Education and Science of the Russian Federation as part of Decree of the Government of the Russian Federation No. 218 dated April 09, 2010.

Acknowledgements
Research were partially conducted at core facility "Structure, mechanical and physical properties of materials".

ABSTRACT

Introduction. Plasma cutting of various metals and alloys is one of the most productive processes for obtaining workpieces, especially when using reverse polarity plasmatrons. The use of plasma cutting in the production of workpieces of large thicknesses potentially allows to increase the productivity of the process. In the domestic industry plasma cutting equipment of foreign production is widely used, which poses the problem of import substitution of manufactured products and equipment with the corresponding parts of Russian companies. For this reason, at present the Institute of Strength Physics and Materials Science together with the company "ITS Siberia" develops plasma cutting equipment on reverse polarity currents. At the same time, in order to determine the peculiarities of influence of parameters and modes of plasma cutting process on the structure of metal in the cutting zone, it is necessary to conduct comparative studies on different metals and alloys. **Aim of the work:** is to identify the characteristics of the influence of high energy impact on the structure and properties of surface layers of aluminum and titanium alloys during plasma cutting using a plasma torch operating with reverse polarity currents. **The research methods** are optical metallography, microhardness measurement and laser scanning microscopy of the surface after plasma cutting. **Results and discussions.** The conducted researches show a wide range of possibilities to adjust the process parameters of plasma cutting of aluminum alloys AA5056 and AA2124, and titanium alloy Grade2. For the alloys used in this work there are optimal values of process parameters, deviations from which lead to various violations of cut quality. Aluminum alloys show a tendency to significant de-strengthening in the cutting zone, which is associated with the formation of a large crystalline structure and large incoherent secondary phases with simultaneous depletion of the solid solution with alloying elements. Titanium alloys are characterized by quenching effects in the cutting zone with increasing microhardness values. Oxides are also formed in the surface layers despite the use of nitrogen shielding gas. In the alloy Ti-4Al-1Mn, in the previously conducted works, the formation of oxide films with high hardness is not noted, while in the Grade2 alloy at cutting in the surface layers oxides are formed sharply increasing the values of microhardness of the material up to values of about 15 GPa. This situation can complicate mechanical processing of titanium alloys after plasma cutting. The obtained results indicate a rather low value of the allowance for further machining after plasma cutting of aluminum and titanium alloys.

For citation: Rubtsov V.E., Panfilov A.O., Knyazhev E.O., Nikolaeva A.V., Cheremnov A.M., Gusarova A.V., Beloborodov V.A., Chumaevskii A.V., Grinenko A.V., Kolubaev E.A. Influence of high-energy impact during plasma cutting on structure and properties of surface layers of aluminum and titanium alloys. *Obrabotka metallov (tekhnologiya, oborudovanie, instrumenty) = Metal Working and Material Science*, 2023, vol. 25, no. 4, pp. 216–231. DOI: 10.17212/1994-6309-2023-25.4-216-231. (In Russian).

*** Corresponding author**
Rubtsov Valery E., Leading researcher
Institute of Strength Physics and Materials Science
of the Siberian Branch of the RAS,
2/4, pr. Akademicheskii,
Tomsk, 634055, Russian Federation
Tel.: +7 (382) 228-68-63, **e–mail:** rvy@ispms.ru

Introduction

Technologies based on the use of plasma effects on the material are widely used for product processing [1], surface modification and coating formation [2], spray coating [3] and many other areas of industrial production of products from metals, alloys, ceramics, polymers and others. The high energy density of the plasma jet allows it to be used both for materials with a high melting point and to increase the productivity of processes associated with it. In particular, the high power of the plasma jet allows it to be used to obtain cut-pieces for subsequent industrial production.

In modern industrial production, plasma cutting, along with laser and waterjet cutting, is one of the most widely used methods for producing metal and alloy cut-pieces [4]. Plasma cutting has the advantage of high productivity and the ability to cut thick sheets [5]. However, despite the widespread use of plasma technology, there are still a number of aspects that require further research. These include reducing the roughness of the cutting surface [6–8], reducing the influence of the cutting process on the structure of the material [9–11], and increasing the productivity and accuracy of the cutting process. In the domestic industry, another task is to obtain analogues of the currently used foreign equipment.

The cut quality can be achieved by optimizing the cutting process parameters [12–14], the most important being the current and the arc voltage [15–17]. The thickness of the sheet used also has a significant influence on the cutting process and the quality of the cut surface [18]. Plasma cutting of heavy plates using direct polarity plasmatrons is potentially difficult due to cathode insert run-out or temperature operation [19, 20], which is especially important in the growing need for import substitution of components. Plasma cutting of rolled sheet using reverse polarity currents is of great importance and potentially allows for a better quality cut surface. In connection with the above, at present "*ITS-Siberia*" and *ISPMS SB RAS* jointly develop modern equipment for plasma cutting at reverse polarity currents. In this case it is important to determine the influence of energy impact during plasma cutting, determined by process parameters, on morphology, structure and mechanical properties of surface layers of billets. Such studies in relation to rolled aluminum and titanium alloy sheets are the purpose of this work.

Materials and methods

Experimental studies were carried out at the production site of *LLC ITS-Siberia* and on the experimental equipment of *ISPMS SB RAS*. The cutting was carried out on a plasmatron with reverse polarity. The scheme of the plasma cutting process is shown in fig. 1, *a*. The general view of the plasma cutting unit is shown in fig. 1, *b*. The unit consists of a worktable, a plasmatron, a gas treatment unit, a moving carriage and guides. In the experiment, the unit with a reverse-polarity plasmatron was used. The cutting of aluminum alloys was performed using plasma gas in the form of air. Nitrogen was used as a shielding and plasma forming gas when cutting titanium alloy.

The cutting of the specimen *1* was performed by a plasma jet *2* formed by an arc between a water-cooled electrode *3* and the inner body of the plasmatron, in which a flow of plasma-forming gas *4* was constantly flowing. For cutting titanium alloy, a shielding gas in the form of nitrogen *5* was used, which was supplied in the outer circuit of the plasmatron. The molten metal *6* was blown out of the cutting zone by the gas flow. As a result of cutting, an area of thermally degraded material (or heat affected zone) *7* and a layer of molten metal (or fusion zone) *8* were formed on the surface of the specimens.

As an experimental material, rolled aluminum alloy *AA2024*, *AA5056* and titanium *Grade2* alloy sheets with a thickness of 10 mm were used. The cutting process parameters used in the study were adjusted to achieve different linear energy of the process. The main cutting parameters were *arc current* and *arc voltage*, which were 170 A and 125 V, respectively. The adjustable parameter was mainly the cutting speed (table).

Metallographic sections were cut from the obtained experimental specimens using the electric discharge sawing (*DK7750* machine) to study the structure and to identify features of changes in the mechanical properties of the near-surface zone. Structural studies were carried out using an *Altami MET 1C* optical microscope and an *Olympus LEXT 4100* laser scanning microscope. Microhardness was determined from the cut surface into the depth of the specimens on metallographic sections using a *Duramin-500* hardness tester.

Results and discussions

Plasma cutting of specimens of aluminum and titanium alloys leads to the formation of a specific relief on the surface, outlining the flow of molten metal displaced by the gas flow from the cutting cavity [18].

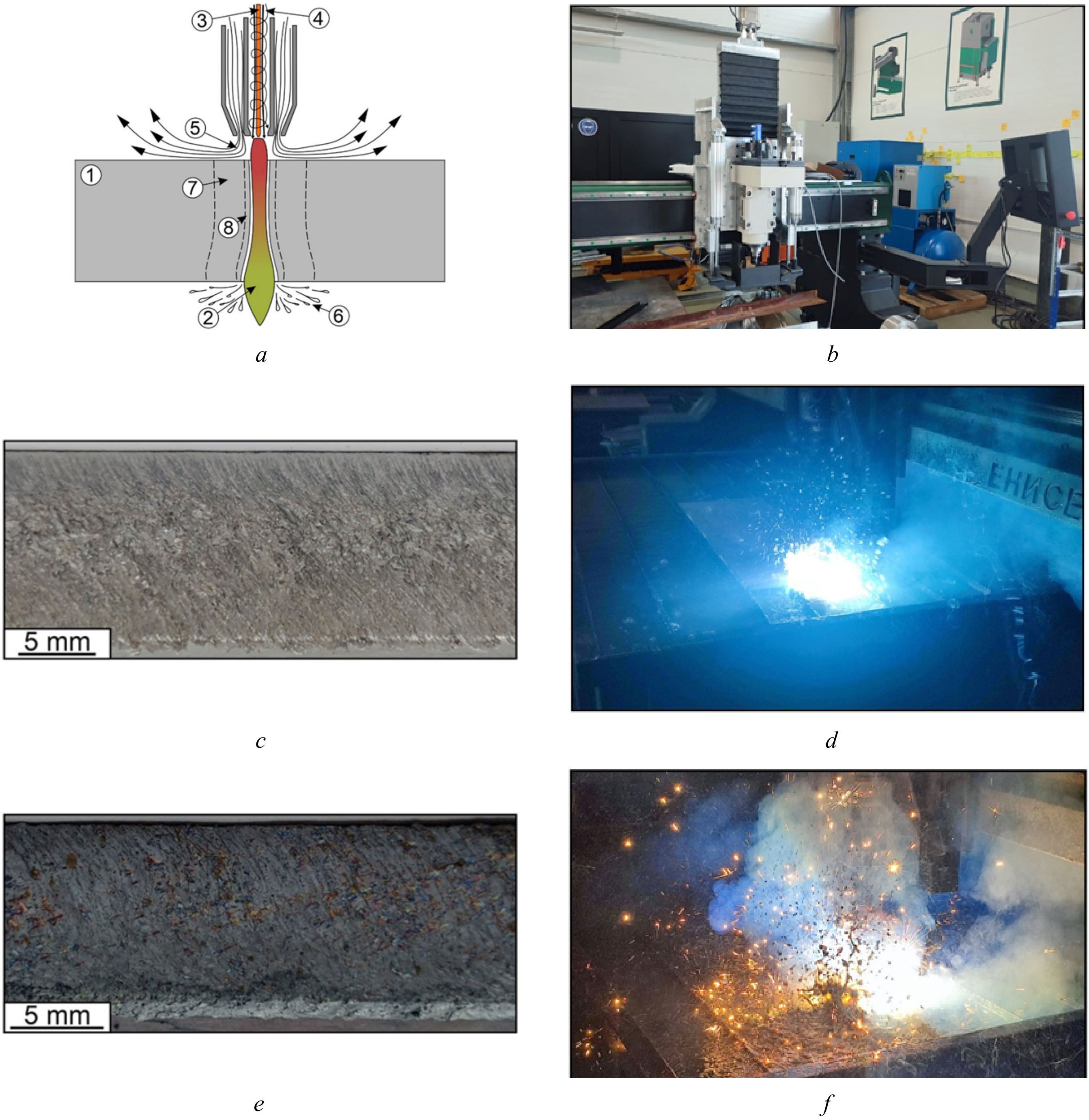

Fig. 1. Plasma cutting of experimental specimens:

plasma cutting flow diagram (*a*); general view of developed setup for plasma cutting (*b*); general view of the cut surface of aluminum alloy *AA2124* (c); general view of the cut surface of *Grade2* titanium alloy (d); image of the cutting process of aluminum alloy *AA2024* (e);image of the cutting process of *Grade2* titanium alloy (f): 1 – blank; 2 – plasma jet; 3 – water-cooled electrode; 4 – plasma-supporting gas; 5 – shielding gas; 6 – material displaced from the cutting zone; 7 – heat affected zone; 8 – surface melting zone

Plasma cutting modes for sheet metal

Alloy	*S*, mm	Mode No.	*I*, A	*U*, V	*V*, m/min	*E*, kJ/m
AA5056	10	1	170	125	3.4	6.3
AA5056	10	2	170	125	3.0	7.1
AA5056	10	3	170	125	2.7	7.9
AA5056	10	4	170	125	3.7	5.7
AA5056	10	5	170	125	4.1	5.2
AA2024	10	1	170	125	4.2	5.1
AA2024	10	2	170	125	3.8	5.6
AA2024	10	3	170	125	3.3	6.4
AA2024	10	4	170	125	4.6	4.6
AA2024	10	5	170	125	5.0	4.3
Grade2	10	1	170	125	4.1	5.2
Grade2	10	2	170	125	3.4	6.3
Grade2	10	3	170	125	3.0	7.1
Grade2	10	4	170	125	2.7	7.9
Grade2	10	5	170	125	2.4	8.9

When cutting specimens of *A5056* alloy with a thickness of 10 mm, such feature led to the formation of a characteristic relief in the lower part of the cut (fig. 2 c, f). The distance between the projections above the cut surface is about 200 μm, the size of the projections is up to 180–200 μm. In the central and upper parts of the cutting area, the relief is more chaotic and characterized by a large size of irregularities.

The size of projections above the surface reaches more than 450–500 μm. Significant differences in the structure of the cutting surface at different modes were not revealed, for the majority of specimens the features of the structure of the cutting surface shown in fig. 2 are preserved. When the *A2024* alloy specimens are cut according to the modes used, no regular relief formation is observed on the surface (fig. 3).

The structure of the cut surface in the upper, central and lower parts of the cut is quite close. The size of the projections above the cut surface is up to 400–450 μm. This structure is also characteristic of most modes and does not change significantly from one specimen to another.

When the *Grade2* alloy specimens are cut, a smoother relief is formed on the cut surface (fig. 4). The average size of the irregularities above the cut surface is up to 200 μm. Although there are differences in the morphology of the cut surface in the upper, lower, and central parts of the cut, it is related more to the orientation of the relief elements than to the size of the irregularities.

The structure of *A5056* alloy specimens (fig. 5) in the surface layers after cutting is mainly represented by the fusion zone (*FZ*) and the heat affected zone (*HAZ*), gradually transitioning to the base metal zone (*BM*). The magnitude of macro distortion of the cut surface varies depends on the mode. The smallest distortion (up to 1,000–1,200 μm) is characteristic of specimens obtained by mode No. 2 at a relatively low (3.0 m/min) cutting speed and above average (7.1 kJ/m) heat input during cutting (fig. 5 a–d). An increase in the cutting speed from these values results in a significant decrease in cut quality, and a decrease in the cutting speed does not result in an increase in cutting accuracy. The depth of the fusion zone is rather small and does not exceed 150 μm from the cutting surface (fig. 5 g, h). The structure in this area is represented by a dendritic structure typical of cast metal, formed during crystallization from the melt. The size of the heat affected zone on the surface of metallographic sections is not revealed, the structure in it is practically identical to the base metal (fig. 5 f–h). This is due to the sufficiently high resistance of the non-heat-treatable ductile aluminum alloy *A5056* to structural changes with increasing temperature.

The structure of the *A2024* alloy specimens after plasma cutting differs significantly from that described above (fig. 6). In this case, the value of macro distortions of the cutting zone reaches a rather significant

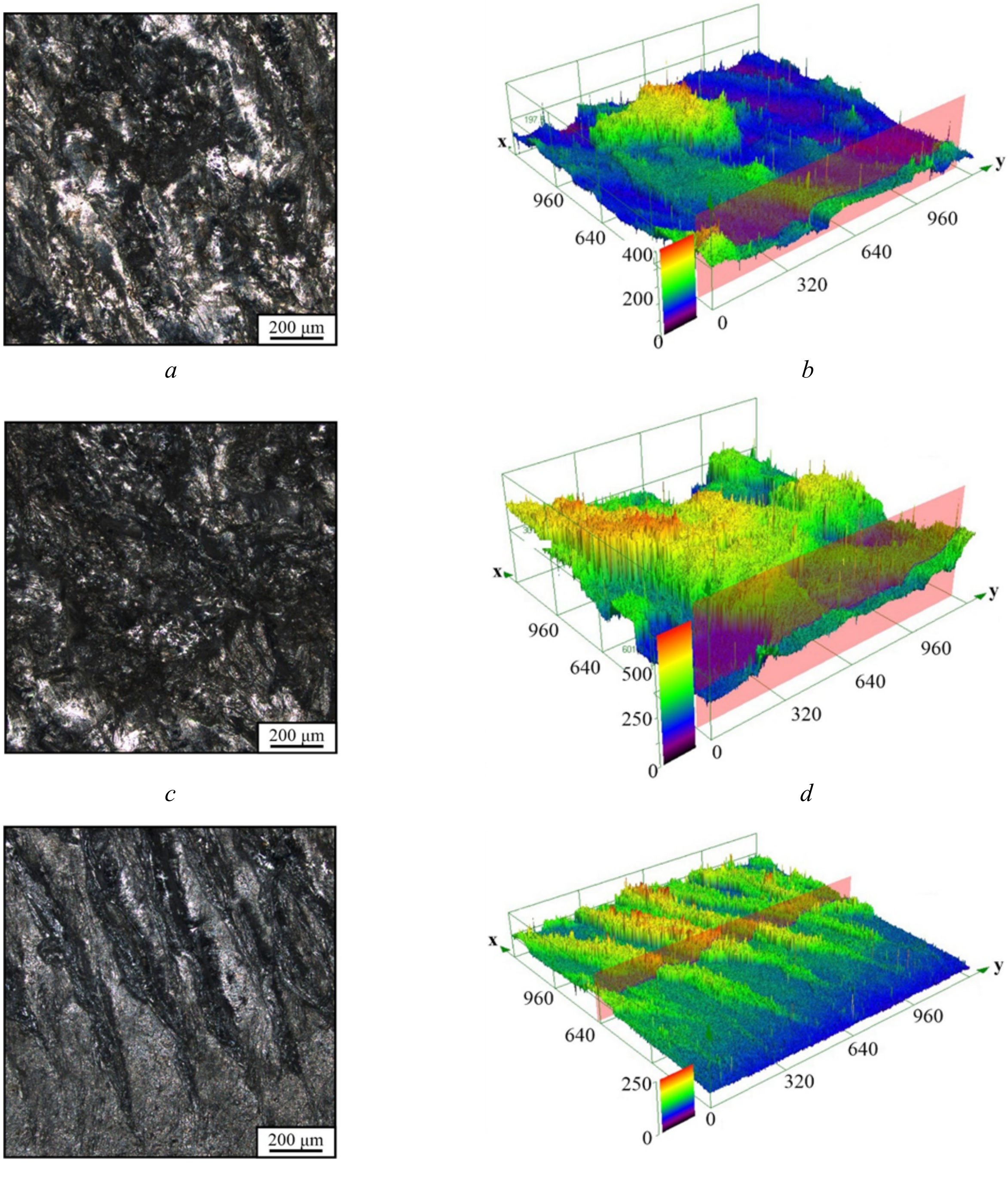

Fig. 2. Surface morphology of *AA5056* alloy specimen after cutting: the upper part of the cut (*a*, *b*); the central part of the cut (*c*, *d*); the lower part of the cut (*e*, *f*); optical images of the surface (*a*, *b*, *c*); 3D images obtained by confocal microscope (*d*, *e*, *f*)

value at high cutting speed in mode No. 5 (fig. 6, *a*–*d*). For other modes, the distortions of the specimen geometry are not so significant. The smallest distortions of the cutting zone (400–450 μm) are characteristic of the specimens obtained by mode No. 4 at a cutting speed of 4.6 m/min and energy input of 4.6 kJ/m.

The size of the fusion zone ranges from 100–150 μm when cutting according to mode No. 4 to 800–1,000 μm when cutting according to mode No. 5. The size of the heat affected zone does not exceed 200–300 μm, which is demonstrated by its increased etchability on metallographic sections. The structure in the fusion zone is represented by a dendritic structure formed during crystallization from the molten state (fig. 6, *g*, *h*). The heat affected zone gradually turns into the base metal with an unchanged structure (fig. 6, *f*, *g*).

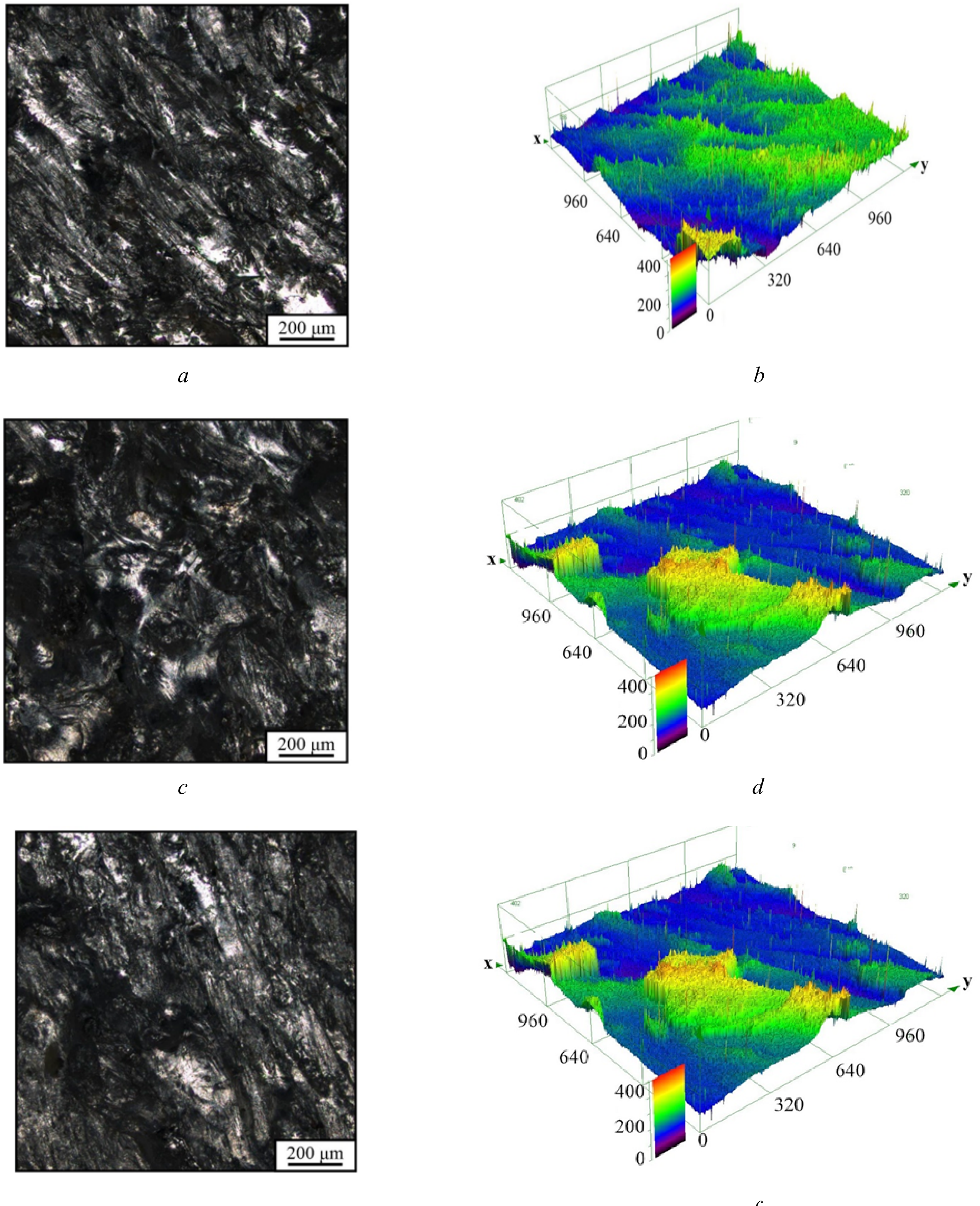

Fig. 3. Surface morphology of AA2024 alloy specimen after cutting: the upper part of the cut (*a*, *b*); the central part of the cut (*c*, *d*); the lower part of the cut (*e*, *f*); optical images of the surface (*a*, *b*, *c*); 3D images obtained by confocal microscope (*d*, *e*, *f*)

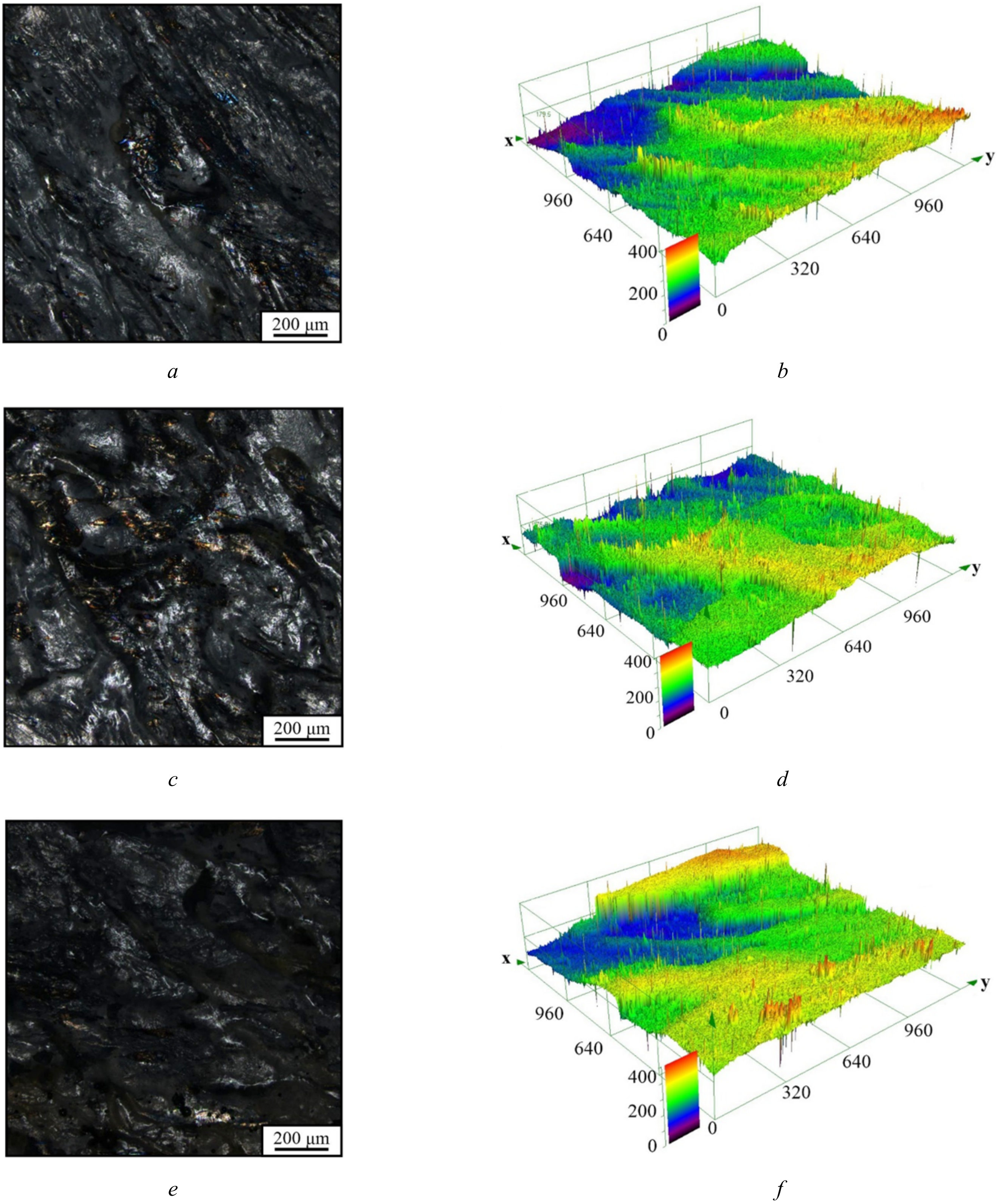

Fig. 4. Surface morphology of *Grade2* titanium alloy specimen after cutting: the upper part of the cut (*a*, *b*); the central part of the cut (c, d); the lower part of the cut (*e*, *f*); optical images of the surface (*a*, *b*, *c*); 3D images obtained by confocal microscope (*d*, *e*, *f*)

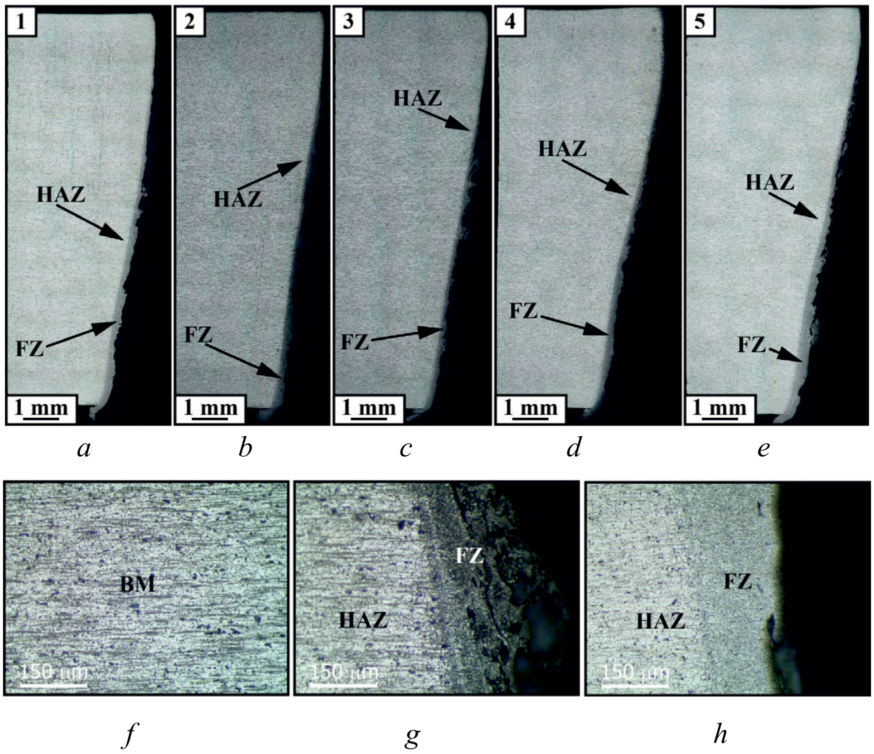

Fig 5. The structure in the cutting zone of the *AA5056* alloy:
the macrostructure of the cut (*a*–*d*); the initial structure of the base material (*f*);
the fusion zones and the heat affected zone (*g*, *h*)

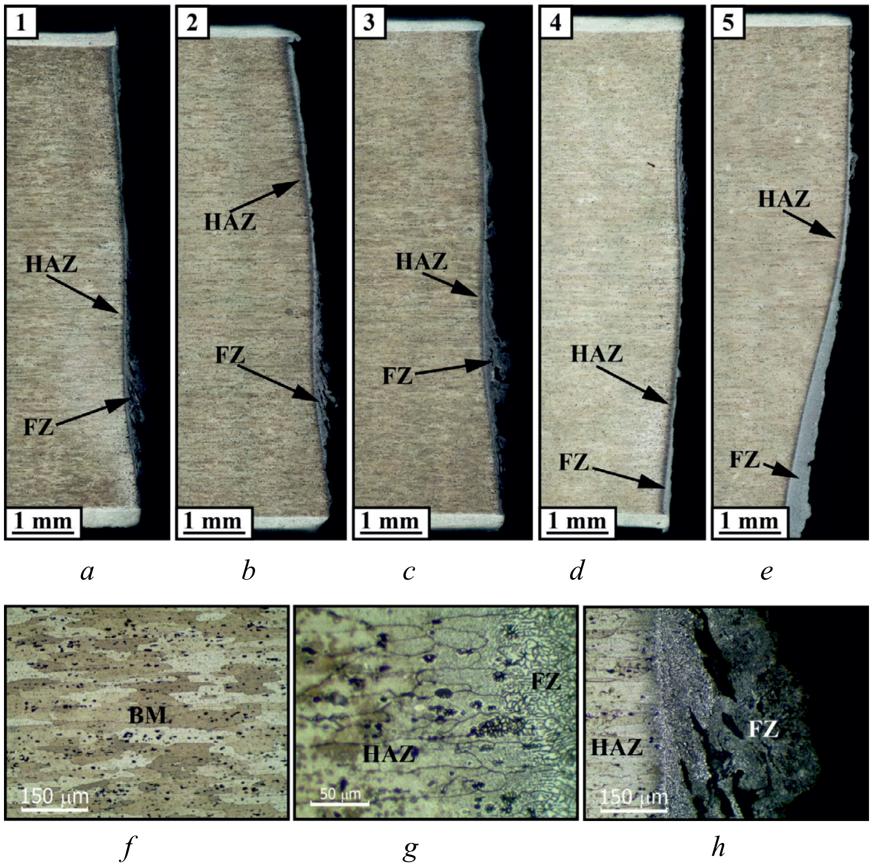

Fig 6. The structure in the cutting zone of the *AA2024* alloy:
the macrostructure of the cut (*a*–*d*); the initial structure of the base material (*f*);
the fusion zones and the heat affected zone (*g*, *h*)

The etchability of the heat affected zone increases as a result of overaging of the material caused by excessive precipitation of alloying elements from the solid solution. This behavior is characteristic of heat treatable alloy *A2024* that is subjected to excessive heat treatment, such as welding.

When cutting specimens of titanium *Grade2* alloy, the structure of the cutting zone is characterized by low values of macro distortions, except for modes No. 1 and No. 5, characterized by the maximum and minimum cutting speed (fig. 7, *a–d*). At an average cutting speed of 3.0 m/min and an energy input of 7.1 kJ/m in mode No. 3, specimens with the smallest deviation of the cut geometry, which is about 450–500 μm, are formed.

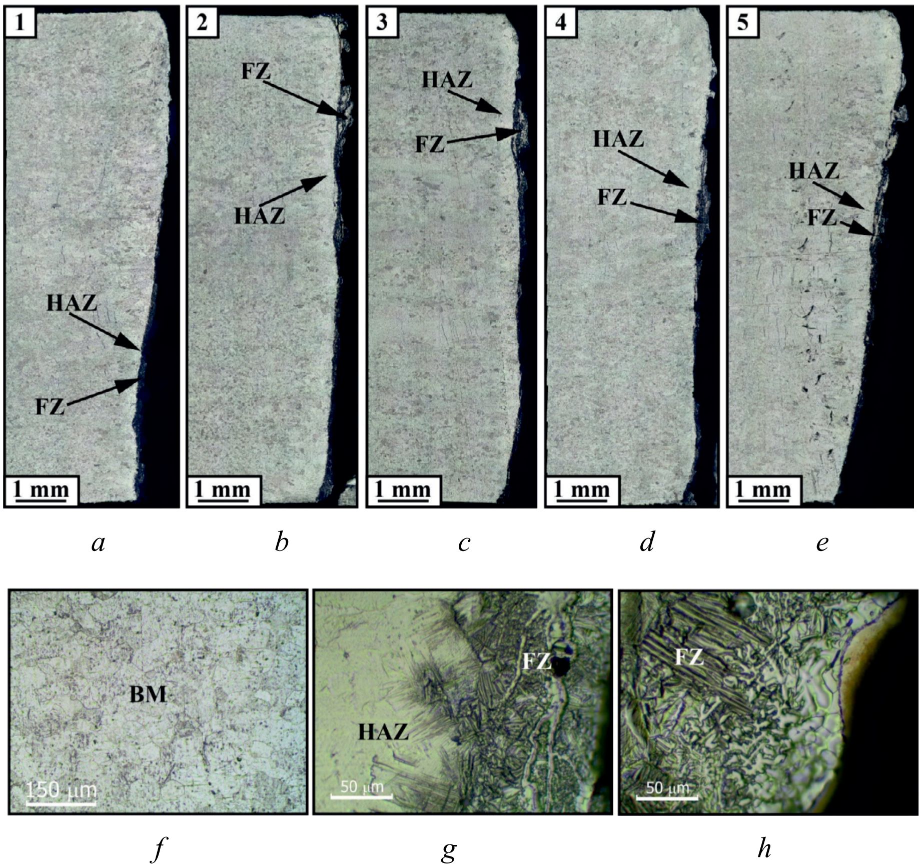

Fig. 7. The structure in the cutting zone of the *Grade2* titanium alloy:
the macrostructure of the cut (*a–d*); the initial structure of the base material (*f*);
the fusion zones and the heat affected zone (*g*, *h*)

The fusion zone for *Grade2* alloy specimens is represented by a dendritic structure (fig. 7, *g*, *h*); its thickness can reach 150–200 μm. The heat affected zone tends to form a needle-like structure (fig. 7, *g*), which significantly differs from the base metal (fig. 7, *f*). However, the heat affected zone for this alloy is rather thin. Closer to the cutting surface of the *Grade2* alloy specimens, thin layers (up to 10 μm thick) are formed (fig. 7, *h*), presumably containing titanium oxides, which, as will be shown later, leads to a sharp increase in the microhardness of the surface layers of the specimens.

Mechanical properties in the cutting zone of the specimens are consistent with structural changes (fig. 8). The *A5056* alloy specimens are characterized by a decrease in microhardness from an average in the base metal of 0.83–0.84 GPa to 0.70–0.75 GPa near the surface in the fusion zone. In the heat affected zone, the microhardness values are intermediate and close enough to the microhardness of the base metal. The total size of the heat affected zone and the fusion zone is about 500–1,000 μm, depending on the cutting mode. For the specimens obtained in optimal mode No. 2, the total value of macro-distortion of the geometry and heat affected zone and fusion zone is about 1,400 μm (1.4 mm), which determines the

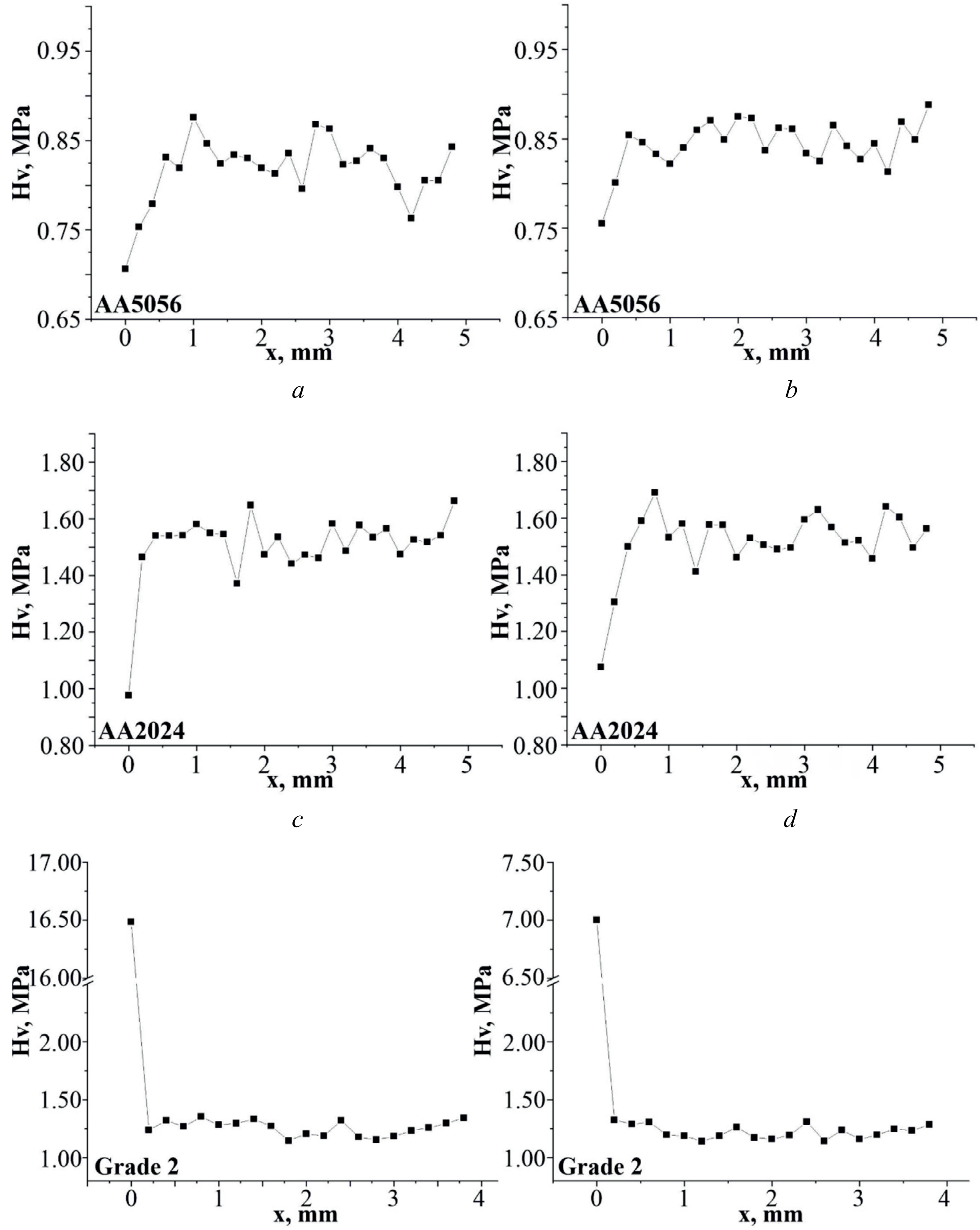

Fig. 8. Changes in microhardness of typical specimens after plasma cutting:
AA5056 alloy (*a*, *b*); *AA2024* alloy (*c*, *d*); *Grade2* titanium alloy (*e*, *f*)

value of the necessary allowance for machining. In the cutting zone of *A2024* alloy specimens, the decrease in microhardness is more significant. With the average microhardness in the base metal zone of 1.52–1.53 GPa, the microhardness in the fusion zone decreases to 0.95–1.05 GPa. At the same time, the total size of the heat affected zone and the fusion zone basically does not exceed 500 μm. For the specimens obtained in optimal mode No. 4, the total size of the heat affected zone and the fusion zone, summarized with the value of the macro distortion of the cutting geometry, is 600 μm (0.6 mm). The *Grade2* alloy is characterized by a sharp increase in microhardness values on average from 1.23–1.24 GPa in the base metal to 7.0–16.5 GPa in the surface layers, indicating the formation of high-hardness titanium oxides. The increase in hardness of the *Ti-2Al-1.5Mn* alloy in the surface layers during cutting [18], which was observed in previous work, is at a much lower level and is due to quenching effects (1.5-fold increase compared to the base metal). The size of the fusion zone and the heat affected zone are at a rather low level. In total, the values of macrogeometric distortion, fusion zone and heat affected zone are about 500 μm (0.5 mm) for *Grade2* alloy when cutting according to the optimum mode No. 3, which determines the smallest of the required allowances for subsequent machining of this alloy.

Conclusion

The influence of high-energy plasma jet impact on the structure and properties of *A5056*, *A2024*, and *Grade2* alloys is expressed in different ways due to its different structure and response to thermal effects. While aluminum alloys are characterized by a decrease in hardness due to thermal degradation of the structure, titanium alloy is characterized by the formation of surface layers with high hardness. The conducted studies show that for the selected alloys, under relatively equal cutting conditions, different cutting parameters and modes are preferable. For alloy *A2024*, modes with minimum heat input are more preferable, while for alloys *A5056* and *Grade2*, modes with average or above average heat input are more suitable. Aluminum alloys are characterized by softening of the near-surface layers of the material during cutting, while titanium alloys are not. In addition, when cutting *Grade2* titanium alloy, oxide layers with hardness significantly (more than 10 times) higher than the hardness of the base metal are formed in the surface layers, which may lead to increased intensity of tool wear during subsequent machining. The *A5056* alloy is characterized by a decrease in microhardness up to 10 % in comparison with the base metal during machining. In the heat affected zone of alloy *A2024*, hardening is significantly higher and is up to 50 % relative to the initial structure of the sheet. Also for these alloys different features of macrogeometry distortion in the cutting zone are observed. *A5056* alloy specimens have the most significant deviations, *A2024* and *Grade2* alloys are characterized by smaller and relatively close values of deviations. Moreover, under the experimental conditions, even with optimal values of cutting parameters, there are still quite significant distortions of the cutting geometry in the *A5056* alloy specimens, which requires further research to improve the quality of the cut. In general, the cutting modes used made it possible to produce billets from *A5056*, *A2024* and *Grade2* alloys with a thickness of 10 mm and with an allowance for subsequent machining of 1.4; 0.6 and 0.5 mm, respectively.

References

1. Murua J., Ibañez I., Dianova A., Domínguez-Meister S., Larrañaga O., Larrañaga A., Braceras I. Tribological and electric contact resistance properties of pulsed plasma duplex treatments on a low alloy steel. *Surface and Coatings Technology*, 2016, vol. 454, p. 129155. DOI: 10.1016/j.surfcoat.2022.129155.

2. Kolubaev A.V., Sizova O.V., Denisova Yu.A., Leonov A.A., Teryukalova N.V., Novitskaya O.S., Byeli A.V. Structure and properties of CrN/TiN multilayer coatings produced by cathodic arc plasma deposition on copper and beryllium-copper alloy. *Physical Mesomechanic*, 2022, vol. 25 (4), pp. 306–317. DOI: 10.1134/S102995992204004X.

3. Wang L., Zhang F., Ma H., He S., Yin F. Microstructure evolution and mechanical properties of plasma sprayed $AlCoCrFeNi_{2.1}$ eutectic high-entropy alloy coatings. *Surface and Coatings Technology*, 2023, vol. 471, p. 129924. DOI: 10.1016/j.surfcoat.2023.129924.

4. Akkurt A. The effect of cutting process on surface microstructure and hardness of pure and Al 6061 aluminium alloy. *Engineering Science and Technology, an International Journal*, 2015, vol. 18 (3), pp. 303–308. DOI: 10.1016/j.jestch.2014.07.004.

5. Ilii S.M., Coteată M. Plasma arc cutting cost. *International Journal of Material Forming*, 2009, vol. 2 (1), pp. 689–692. DOI: 10.1007/s12289-009-0588-4.

6. Bini R., Colosimo B.M., Kutlu A.E., Monno M. Experimental study of the features of the kerf generated by a 200A high tolerance plasma arc cutting system. *Journal of Materials Processing Technology*, 2008, vol. 196 (1–3), pp. 345–355. DOI: 10.1016/j.jmatprotec.2007.05.061.

7. Patel P., Nakum B., Abhishek K., Rakesh Kumar V., Kumar A. Optimization of surface roughness in plasma arc cutting of AISID2 steel using TLBO. *Materials Today: Proceedings*, 2018, vol. 5, iss. 9 (3), pp. 18927–18932. DOI: 10.1016/j.matpr.2018.06.242.

8. Hoult A.P., Pashby I.R., Chan K. Fine plasma cutting of advanced aerospace materials. *Journal of Materials Processing Technology*, 1995, vol. 48 (1–4), pp. 825–831. DOI: 10.1016/0924-0136(94)01727-I.

9. Nandan Sharma D., Ram Kumar J. Optimization of dross formation rate in plasma arc cutting process by response surface method. *Materials Today: Proceedings*, 2020, vol. 32 (3), pp. 354–357. DOI: 10.1016/j.matpr.2020.01.605.

10. Gariboldi E., Previtali B. High tolerance plasma arc cutting of commercially pure titanium. *Journal of Materials Processing Technology*, 2005, vol. 160 (1), pp. 77–89. DOI: 10.1016/j.jmatprotec.2004.04.366.

11. Gostimirović M., Rodić D., Sekulić M., Aleksić A. An experimental analysis of cutting quality in plasma arc machining. *Advanced Technologies & Materials*, 2020, vol. 45 (1), pp. 1–8. DOI: 10.24867/ATM-2020-1-001.

12. Cinar Z., Asmael M., Zeeshan Q. Developments in plasma arc cutting (PAC) of steel alloys: A review. *Jurnal Kejuruteraan*, 2018, vol. 30 (1), pp. 7–16. DOI: 10.17576/jkukm-2018-30(1)-02.

13. Kudrna L., Fries J., Merta M. Influences on plasma cutting quality on CNC machine. *Multidisciplinary Aspects of Production Engineering*, 2019, vol. 2 (1), pp. 108–117. DOI: 10.2478/mape-2019-0011.

14. Anakhov S.V., Guzanov B.N., Matushkin A.V., Pugacheva N.B., Pykin Y.A. Vliyanie konstruktivnykh osobennostei plazmotrona na kachestvo reza pri pretsizionnoi vozdushno-plazmennoi razdelke metalla [Influence of plasma torch design on cutting quality during precision air-plasma cutting of metal]. *Izvestiya vysshikh uchebnykh zavedenii. Chernaya Metallurgiya = Izvestiya. Ferrous Metallurgy*, 2020, vol. 63 (2), pp. 155–162. DOI: 10.17073/0368-0797-2020-2-155-162.

15. Peko I., Marić D., Nedić B., Samardžić I. Modeling and optimization of cut quality responses in plasma jet cutting of aluminium alloy EN AW-5083. *Materials*, 2021, vol. 14 (19), p. 5559. DOI: 10.3390/ma14195559.

16. Salonitis K., Vatousianos S. Experimental investigation of the plasma arc cutting process. *Procedia CIRP*, 2012, vol. 3, pp. 287–292. DOI: 10.1016/j.procir.2012.07.050.

17. Suresh A., Diwakar G. Optimization of process parameters in plasma arc cutting for TWIP steel plates. *Materials Today: Proceedings*, 2021, vol. 38 (5), pp. 2417–2424. DOI: 10.1016/j.matpr.2020.07.383.

18. Rubtsov V.E., Panfilov A.O., Knyazhev E.O., Nikolaeva A.V., Cheremnov A.M., Gusarova A.V., Beloborodov V.A., Chumaevskii A.V., Ivanov A.N. Otrabotka metodiki plazmennoi rezki medi marki M1, alyuminievogo splava D16T i titanovogo splava OT4-1 s ispol'zovaniem plazmotrona s obratnoi polyarnost'yu [Development of plasma cutting technique for C1220 copper, AA2024 aluminum alloy, and Ti-1,5Al-1,0Mn titanium alloy using a plasma torch with reverse polarity]. *Obrabotka metallov (tekhnologiya, oborudovanie, instrumenty) = Metal Working and Material Science*, 2022, vol. 24, no. 4, pp. 33–52. DOI: 10.17212/1994-6309-2022-24.4-33-52.

19. Matushkina I., Anakhov S., Pyckin Yu. Design of a new gas-dynamic stabilization system for a metal-cutting plasma torch. *Journal of Physics: Conference Series*, 2021, vol. 2094, p. 042075. DOI: 10.1088/1742-6596/2094/4/042075.

20. Shchitsyn V.Yu., Yazovskikh V.M. Effect of polarity on the heat input into the nozzle of a plasma torch. *Welding International*, 2002, vol. 16 (6), pp. 485–487. DOI: 10.1080/09507110209549563.

Conflicts of Interest

The authors declare no conflict of interest.